



Research article

Arrhenius kinetics driven nonlinear mixed convection flow of Casson liquid over a stretching surface in a Darcian porous medium

N. Vishnu Ganesh^a, Qasem M. Al-Mdallal^{b,*}, R. Kalaivanan^c, K. Reena^d^a PG and Research Department of Mathematics, Ramakrishna Mission Vivekananda College, Mylapore, Chennai, 600004, Tamil Nadu, India^b Department of Mathematical Sciences, United Arab Emirates University, P.O. Box 15551, Al Ain, Abu Dhabi, United Arab Emirates^c Department of Mathematics, Vivekananda College, Madurai, 625234, Tamil Nadu, India^d Department of Mathematics, Nehru Arts and Science College, Coimbatore, 641105, Tamil Nadu, India

ARTICLE INFO

Keywords:

Arrhenius kinetics
Casson liquid
Darcian porous medium
Nonlinear mixed convection
Stretching surface

ABSTRACT

The non-linear mixed convective heat and mass transfer features of a non-Newtonian Casson liquid flow over a stretching surface are investigated numerically. The stretching surface is embedded in a Darcian porous medium with heat generation/absorption impacts. The fluid flow is assumed to be driven by both buoyancy and Arrhenius kinetics. The governing equations are modelled with the help of Boussinesq and Rosseland approximations. The similarity solutions of the non-dimensional equations are obtained using two numerical approaches, namely fourth fifth Runge - Kutta Fehlberg method and the shooting approach. The velocity, temperature and concentration profiles are discussed for important physical parameters through various graphical illustrations. The skin friction, the non-dimensional wall temperature, and the concentration expressions were derived and analysed. The results indicate that the increasing values of linear and nonlinear convection due to temperature, nonlinear convection due to concentration, and heat of reaction increase the dimensionless wall temperature. The dimensionless wall concentration rises with the increasing values of heat of reaction, linear and nonlinear convection due to temperature, and nonlinear convection due to concentration parameters.

1. Introduction

The fluid flow along with heat and mass transport in a porous medium has gained major attention of researchers in the previous few decennaries. The thermo-physical properties of the fluid and the features of the permeability of the porous medium possess a primary role in controlling the performance of heat and mass transfer in fluids. The number of research studies in this topic has increased because of its various engineering applications, such as geophysical, crystal growth in fluids, pollutant dispersion in aquifers, petroleum reservoirs, nuclear waste repositories, chemical catalytic reactors, ground hydrology, solidification of casting, thermal and insulating engineering, etc. To predict the fluid flow in a porous space, the law of Darcy has been widely used by researchers [1]. The law of Darcy is a proportional relationship between the viscosity of fluid, the immediate expulsion rate through porous space, and the pressure drop over a certain distance. It is valid only for laminar, viscous, and slow fluid flow where the inertial effects are neglected.

* Corresponding author.

E-mail addresses: nvishnuganeshmath@gmail.com (N.V. Ganesh), q.almdallal@uaeu.ac.ae (Q.M. Al-Mdallal).<https://doi.org/10.1016/j.heliyon.2023.e16135>

Received 23 November 2022; Received in revised form 24 April 2023; Accepted 7 May 2023

Available online 18 May 2023

2405-8440/© 2023 The Authors. Published by Elsevier Ltd. This is an open access article under the CC BY-NC-ND license (<http://creativecommons.org/licenses/by-nc-nd/4.0/>).

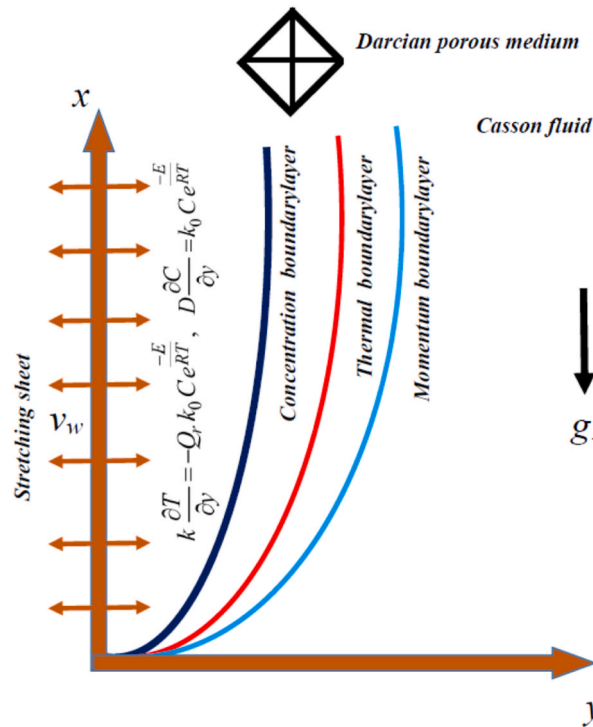


Fig. 1. Physical configuration of the present problem.

The advancement in porous medium studies has been summarised in the following books [2–6].

Non-Newtonian liquids are liquids that exhibit a nonlinear relationship among the shear rate and shear stress. The rheological behaviour of these liquids plays a dynamic role in many cosmetic, pharmaceutical, and chemical industries. It is very difficult to derive a single model to predict non-Newtonian liquids due to the nonlinear relationship between stress and strain movement. Several researchers have developed various mathematical models of non-Newtonian liquids, such as Walter-B [7,8], Maxwell [9], viscoelastic type [10], Casson [11], Brinkman type [12], Jeffrey [13], power law [14], second-grade [15] model, Bingham plastic [16], and Oldroyd-B [17]. Casson liquid is a subset of a non-Newtonian model that acts like an elastic solid. These liquids have infinite viscosity at zero shear rate as well as infinite shear rate at zero viscosity. Human blood, concentrated juices, honey, and lubricants are some of the Casson liquid examples [18]. The Casson property of the fluids is also important in industrial processes such as coating, manufacturing, metal spinning, biomimetics, etc. In addition to this, the theoretical investigations on mixed convection flow of non-Newtonian fluids over a stretching material problem might have enormous economic and energy saving implications for the industries that involve extrusion of molten polymers, hot rolling, food stuffs processing, paper production, and glass fibre production. The Newtonian/non-Newtonian fluid flow problems over a stretching surface in a porous medium have attracted many researchers in recent years [19–24].

Bhattacharyya [25] examined the two-dimensional stagnation point flow of Casson liquid towards a stretching surface with magnetic field effects and found that Casson fluid has a thicker velocity boundary layer than Newtonian fluid. Shehzad et al. [26] investigated the 3D (three-dimensional) flow of Casson liquid in a Darcian porous medium with a uniform heat source/sink and magnetic field effects. Their investigation showed that a greater Casson value increased the skin friction coefficient. Mabood et al. [27] inspected the Casson liquid flow under MHD effects in a Darcian porous medium, taking into account of melting heat transfer and radiation, and reported that the Casson parameter enhances the heat transfer rate. The impacts of cross diffusion and a heat source on the boundary layer flow of Casson liquid in the porous medium in the presence of non-linear thermal radiation were analysed by Patel [28]. The same author [29] studied the Casson liquid flow over an oscillating plate embedded in a porous space under the effects of heat generation, hall current, and radiation. The heat and mass transport characteristics of Casson liquid over a shrinking sheet in a porous medium in the presence of a heat source/sink were examined by Awais et al. [30]. Nandkeolyar and Chamkha [31] analysed the unsteady Casson liquid flow in three-dimensional stretching material in a porous medium with Hall and MHD effects. Eldabe et al. [32] discussed the impacts of the electromagnetic field on the heat and mass transfer of Casson liquid in a porous medium.

The present study mainly focused on the mixed convection flow of Casson liquid, which is purely driven by the heat provided to the fluid due to exothermic surface reactions and non-uniform internal heat generation/absorption over a stretching surface in a Darcian porous medium. The exothermic reactions were derived and utilised by the following researchers [33–38]. The derived model was dependent on the Arrhenius temperature and a first order kinetics. The forth mentioned model was successfully applied to the boundary layer flow problems over a stretching sheet [39–45]. Very recently, the second grade nanofluid boundary layer flow was

investigated over a stretching surface that was driven by Arrhenius kinetics [46].

To the best of the author’s knowledge, the problem of nonlinear mixed convection flow of Casson liquid over a stretching surface in a porous medium driven by Arrhenius kinetics, which has applications in many engineering processes as mentioned earlier, has not been considered yet. Hence in the present work, Arrhenius kinetically driven boundary layer flow of non-Newtonian Casson liquid over a stretching surface in a Darcian porous medium with the impacts of thermal radiation, non-uniform heat generation, and heat absorption. The numerical results are obtained for the governing equations through the fourth fifth Runge-Kutta Fehlberg method along with shooting technique. The results are discussed through graphical illustrations.

2. Problem formulation

We consider the steady, incompressible, two-dimensional, nonlinear mixed convection flow of a non-Newtonian Casson liquid over a stretching surface that is embedded in a porous medium. The porous medium is considered as a Darcian porous medium. The impacts of space and temperature dependent heat generation/absorption, and Rosseland thermal radiation impacts are taken into account with negligible viscous dissipation impacts. Flow is assumed to be happening in a cartesian framework in which the x axis is taken along the surface and the y axis vertical to it (Fig. 1). The stretching surface is assumed to be at temperature T_w (ambient temperature T_∞) and concentration C_w (ambient concentration C_∞) with stretching velocity $u_w = a/x^{-1}$. The exothermic reaction is presumed to take place at the surface.

The governing equations can be written under the above and Boussinesq assumptions as [27–30].

$$\left(\frac{\partial u}{\partial x}\right) + \left(\frac{\partial v}{\partial y}\right) = 0, \tag{1}$$

$$\begin{aligned} \frac{\partial u}{\partial x} u + v \frac{\partial u}{\partial y} = & \frac{\vartheta}{\beta_1} \frac{\partial^2 u}{\partial y^2} (\beta_1 + 1) + g_1 [\beta_{t2}(T - T_\infty)^2 + \beta_{t1}(T - T_\infty)] \\ & + g_1 [\beta_{c2}(C - C_\infty)^2 + \beta_{c1}(C - C_\infty)] - \vartheta \left(1 + \frac{1}{\beta_1}\right) \left(\frac{k_p}{u}\right)^{-1}, \end{aligned} \tag{2}$$

$$\rho c_p \left(\frac{\partial T}{\partial x} u + v \frac{\partial T}{\partial y}\right) = \frac{\partial^2 T}{\partial y^2} k + Q_{ST} - \frac{\partial q_r}{\partial y}, \tag{3}$$

$$\frac{\partial C}{\partial x} u + v \frac{\partial C}{\partial y} = \frac{\partial^2 C}{\partial y^2} D. \tag{4}$$

Where u and v are the velocity components along x and y axes respectively, β_1 is the Casson parameter, ϑ is the kinematic viscosity, g_1 is acceleration due to gravity, β_{t1} is first order thermal expansion coefficient, β_{t2} is second order thermal expansion coefficient, β_{c1} is the first order solutal coefficient, β_{c2} is the second order solutal coefficient, T is the temperature of the fluid, k_p is the permeability of the porous medium, ρ is the density of the Casson liquid, k is the thermal conductivity, C_p is the specific heat capacitance, C is the concentration of fluid, and D is the molecular diffusion coefficient.

The non-uniform heat generation/absorption can be chosen as [47].

$$Q_{ST} = u_w [(T_w - T_\infty) Q_1 + Q_2 (T - T_\infty)] \left(\frac{\vartheta x}{k}\right)^{-1}, \tag{5}$$

where Q_1 is the parameter for space dependent heat generation/absorption and Q_2 is the parameter for temperature dependent heat generation/absorption. It should be mentioned here that $Q_1 < 0$ and $Q_2 < 0$ represent the heat absorption case, while $Q_1 > 0$ and $Q_2 > 0$ represent the heat generation case.

Utilising the linear Rosseland formulation for radiative heat flux q_r , which can be defined as [27].

$$q_r = -\frac{4}{3} \left(\frac{\partial T^4}{\partial y}\right) \left(\frac{k_{ab}}{\sigma_{sb}}\right)^{-1}, \tag{6}$$

where σ_{sb} is the constant of Stefan-Boltzmann and k_{ab} is the coefficient of mean absorption. The 4th power of temperature can be expressed as a linear function of temperature as follows:

$$T^4 = -3T_\infty^4 + 4T_\infty^3 T. \tag{7}$$

Invoking eqs (5)–(7) in (3), we get

$$\begin{aligned} \rho c_p \left(\frac{\partial T}{\partial x} u + v \frac{\partial T}{\partial y}\right) = & \frac{\partial^2 T}{\partial y^2} k + u_w [(T_w - T_\infty) Q_1 + Q_2 (T - T_\infty)] \left(\frac{\vartheta x}{k}\right)^{-1} \\ & + \frac{16}{3} T_\infty^3 \left(\frac{\partial^2 T}{\partial y^2}\right) \left(\frac{k_{ab}}{\sigma_{sb}}\right)^{-1} \end{aligned} \tag{8}$$

The boundary conditions for the catalytic surface are [40–46].

$$u - u_w = 0, v - v_w = 0, k \frac{\partial T}{\partial y} = -Q_r e^{\frac{-E}{RT}} (k_0 C) \text{ and } \frac{\partial C}{\partial y} = k_0 e^{\frac{-E}{RT}} \left(\frac{C}{D}\right), \text{ at } y = 0,$$

$$u \rightarrow 0, T \rightarrow T_\infty, C \rightarrow C_\infty, \text{ as } y \rightarrow \infty. \tag{9}$$

Where E is the activation energy Q_r is the exothermicity of reaction and R is gas constant.

By introducing the following dimensionless transformations [46]

$$u = g'(\zeta)ax, v = -g(\zeta)(a\theta)^{1/2}, \zeta = y\left(\frac{\theta}{a}\right)^{-1/2},$$

$$\theta(\zeta) = \left(\frac{E}{R}\right)\left(\frac{1}{T_\infty^2}\right)(T - T_\infty) \text{ and } \varphi(\zeta) = \left(\frac{1}{C_\infty}\right)(C - C_\infty), \tag{10}$$

the governing equations in (2)-(4) and (8) are transformed into the following dimensionless form and also the transformations in (10) satisfies the continuity eq. (1),

$$(\beta_1^{-1} + 1)g''' + g g'' + (1 + \lambda_{t2} \theta)\theta\lambda_{t1} + \lambda_{c1} \varphi(1 + \lambda_{c2} \varphi) = g'2 + g'k_1(\beta_1^{-1} + 1), \tag{11}$$

$$\left(1 + \frac{4}{3N^{-1}}\right)\theta'' + \text{Pr} \theta' g + g' Q_1 + Q_2 \theta = 0, \tag{12}$$

$$\varphi'' + \varphi' g Sc = 0, \tag{13}$$

Consequently, the corresponding boundary conditions in (9) become

$$g(0) = s, g'(0) = 1, g'(\infty) = 0, \frac{\theta'(0)}{(1 + \varphi(0))} = -e^{\left(\frac{\theta(0)}{1 + \varepsilon \theta(0)}\right)} \alpha \text{ and } \theta(\infty) = 0, \frac{\varphi'(0)}{(1 + \varphi(0))} = e^{\left(\frac{\theta(0)}{1 + \varepsilon \theta(0)}\right)} \beta \text{ and } \varphi(\infty) = 0. \tag{14}$$

Where $\lambda_{t1} = \left(\frac{R}{E}\right)\left(\frac{T_\infty^2 \beta_{t1}}{u_w}\right)\left(\frac{g_1}{a}\right)$ is the mixed convection parameter due to temperature, $\lambda_{t2} = \left(\frac{R}{E}\right)\left(\frac{\beta_{t2}}{\beta_{t1}}\right)T_\infty^2$ is the nonlinear convection parameter due to temperature, $\lambda_{c1} = C_\infty\left(\frac{\beta_{c1}}{u_w}\right)T_\infty^2$ is the mixed convection parameter due to concentration, $\lambda_{c2} = \left(\frac{\beta_{c2}}{\beta_{c1}}\right)C_\infty$ is the nonlinear convection parameter due to concentration, $k_1 = \frac{1}{k_p a}\left(\frac{\mu}{\rho}\right)$ is the porous medium parameter, $N = 4\left(\frac{\sigma_{sb}}{k_{ab}}\right)\left(\frac{1}{k}\right)T_\infty^3$ is the radiation parameter, $\text{Pr} = \left(\frac{\theta}{a}\right)$ is the Prandtl number, $Sc = \left(\frac{D}{\theta}\right)$ is the Schmidt number, $\alpha = \frac{Q_k \Omega}{k_c} \left(\frac{E}{R}\right) e^{\frac{-E}{RT_\infty}} \sqrt{\frac{\theta}{a}} \left(\frac{C_\infty}{T_\infty}\right)$ is the heat of reaction parameter, $\beta = \left(\frac{1}{D}\right)k_0 e^{\frac{-E}{RT_\infty}} \sqrt{\frac{\theta}{a}}$ is the reaction rate and $\varepsilon = \left(\frac{R}{E}\right)T_\infty$ is the activation energy parameter.

3. Physical quantities of attention

The physical quantities on which present research focuses are the skin friction coefficient, non-dimensional wall temperature and non-dimensional wall concentration.

The shear stress at the surface of the wall is given by

$$\tau_w = \mu(\beta_1^{-1} + 1) \left(\frac{\partial u}{\partial y}\right)_{y=0}$$

The skin friction coefficient C_f can be defined as

$$C_f = \frac{\tau_w}{\rho u_w^2} = \frac{\mu(\beta_1^{-1} + 1) \left(\frac{\partial u}{\partial y}\right)_{y=0}}{\rho u_w^2}.$$

$$\text{Re}_x^{1/2} C_f = g''(0)(\beta_1^{-1} + 1).$$

The non-dimensional wall temperature and wall concentration can be obtained from the following equations.

$$T_w = T_\infty + \left(\frac{R}{E}\right)T_\infty^2 \theta(0) \text{ and } C_w = C_\infty + C_\infty \varphi(0).$$

Table 1

Comparison of $-\theta'(0)$ in the absence of β_1 and $\alpha=0, \beta=0, N=0, k_1=0, Q_1=0, Q_2=0, \mathcal{E}=0, \lambda_{t1}=0, \lambda_{t2}=0, \lambda_{c1}=0, \lambda_{c2}=0$ and $Sc = 0$ with boundary condition $\theta(0) = 1$ and $\theta(\infty) = 0$.

Pr	Khan and Pop [48]	Ullah et al. [49]	Present results
0.7	0.4539	0.4544	0.45391620
2.0	0.91130	0.9113	0.91135764
7.0	1.8954	1.8953	1.89540326
20.0	3.3539	3.3538	3.35390651

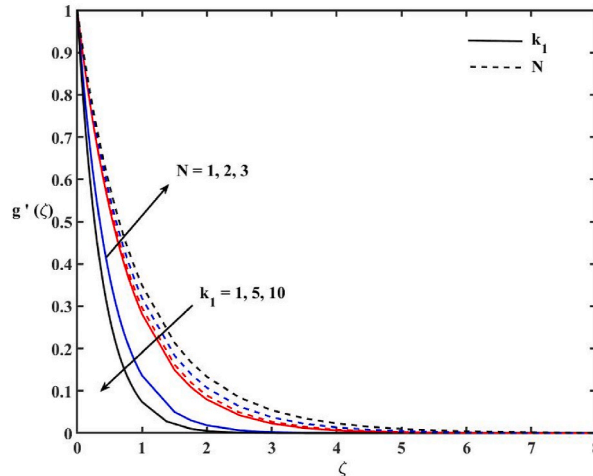


Fig. 2. Effects of N and k_1 on velocity profile.

4. Method of solution

The governing eqs (11)–(13) along with the boundary conditions in (14) are numerically solved using fourth fifth Runge-Kutta Fehlberg integration scheme along with the shooting iteration approach. Runge-Kutta Fehlberg method is a numerical scheme of order two with an error estimator of order 5 that is used to solve ordinary differential equations. The steps involved in the numerical procedure are as follows:

First the boundary value problem is transformed into the following first order initial value problem:

$$\begin{aligned}
 y_1' = y_2, y_2' = y_3, y_3' &= \frac{[y_2^2 - y_1 y_3 - \lambda_{t1} y_4 (1 + \lambda_{t2} y_4) - \lambda_{c1} y_6 (1 + \lambda_{c2} y_6) + k_1 (\beta_1^{-1} + 1) y_2]}{(\beta_1^{-1} + 1)} \\
 y_4' = y_5, y_5' &= \frac{[-Pr y_1 y_5 - Q_1 y_2 - Q_2 y_4]}{(1 + \frac{4}{3N-1})}, y_6' = y_7, y_7' = -Sc y_1 y_7.
 \end{aligned}
 \tag{18}$$

with the boundary conditions

$$\begin{aligned}
 y_1(0) = s, y_2(0) = 1, y_3(0) = \text{guess}_1, y_4(0) = \text{guess}_2, y_5(0) = -\alpha(1 + y_6(0)) e^{\left(\frac{y_4(0)}{1+\epsilon y_4(0)}\right)}, \\
 y_6(0) = \text{guess}_3, y_7(0) = \beta(1 + y_6(0)) e^{\left(\frac{y_4(0)}{1+\epsilon y_4(0)}\right)}.
 \end{aligned}
 \tag{19}$$

The initial guesses ($\text{guess}_1, \text{guess}_2$ and guess_3) are chosen, and the Runge Kutta Fehlberg method is used to integrate the first order systems. Then the computed values are compared with the boundary conditions. The shooting method is used to update the initial guesses to satisfy the boundary conditions, and the process is repeated until the results reach the preferred accuracy of 10^{-6} .

5. Results and discussion

The set of first order ordinary differential eq. (18) and the corresponding initial conditions (19) with guess values are numerically solved using the Runge - Kutta Fehlberg method along with the shooting approach. The present numerical code is validated with those

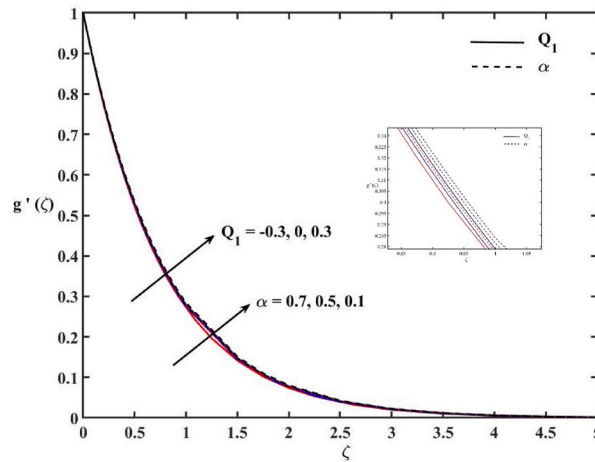


Fig. 3. Effects of Q_1 and α on velocity profile.

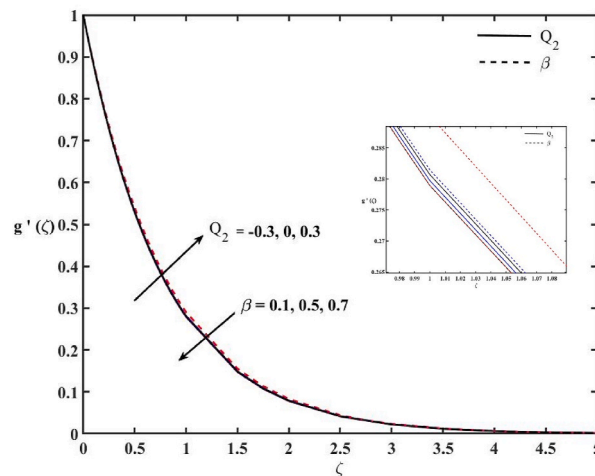


Fig. 4. Effects of Q_2 and β on velocity profile.

of Khan and Pop [48] and Ullah et al. [49]. The comparison results are tabulated in Table 1. An excellent agreement is observed in the $-\theta'(0)$ values for various Prandtl numbers in the absence of β_1 and $\alpha = 0, \beta = 0, N = 0, k_1 = 0, Q_1 = 0, Q_2 = 0, \mathcal{E} = 0, \lambda_{t1} = 0, \lambda_{t2} = 0, \lambda_{c1} = 0, \lambda_{c2} = 0$ and $Sc = 0$. The impacts of the radiation parameter (N), porous medium parameter (k_1), space dependent heat generation/absorption parameter (Q_1), temperature dependent heat generation/absorption parameter (Q_2), heat of reaction parameter (α), reaction rate parameter (β), Casson parameter (β_1) and activation energy parameter (\mathcal{E}) on Casson liquid velocity, temperature, and concentration profiles are plotted in Fig. 2–13. The variation of skin friction, non-dimensional wall temperature, and concentration are illustrated in Figs. 14–16. We fixed $Pr = 3, \beta_1 = 1, \alpha = 0.5, \beta = 0.5, N = 1, k_1 = 1, Q_1 = 0.5, Q_2 = 0.5, \mathcal{E} = 0.5, \lambda_{t1} = 0.5, \lambda_{t2} = 0.3, \lambda_{c1} = 0.4, \lambda_{c2} = 0.5$ and $Sc = 1$ throughout the investigation when studying a particular parameter. It is worth mentioning that when $\beta_1 \rightarrow \infty$, the present Casson liquid model is reduced to a Newtonian liquid case, the present problem is also reduced to a problem of Casson liquid flow over a flat catalytic surface when $\lambda_{t1} = 0$ and $\lambda_{c1} = 0$.

Due to the presence of concentration and thermal buoyancies in the momentum Eq. (11), the parameters $N, Q_1, Q_2, \alpha, \beta,$ and \mathcal{E} have influence on the velocity profile of the Casson liquid. The combined impacts of N and k_1 on the Casson liquid velocity profile are represented in Fig. 2. Both N and k_1 show significant impacts on velocity profile ($g'(\zeta)$). It is observed that the increase in N accelerates the velocity profile while the enhancement in k_1 decelerates the velocity profile of the Casson liquid. This is because the increase in N enhances the velocity boundary layer thickness. The parameter k_1 is related to the sizes of pores. From the definition of parameter k_1 , one may see that the increase of k_1 leads to a decrease in the size of pores, which causes higher resistance to the Casson liquid flow inside the porous medium. Consequently, the velocity profile decreases with k_1 . Fig. 3 reveals the impacts α and Q_1 on $g'(\zeta)$. The positive value of Q_1 denotes the presence of space dependent heat generation while the negative value denotes space dependent heat absorption. Both Q_1 and α do not show a significant impact on $g'(\zeta)$. A slight growth in the $g'(\zeta)$ is traced when $Q_1 > 0$, and a reverse trend is observed and felt when $Q_1 < 0$. The reason for this is that the velocity boundary layer thickness reduces in the heat absorption

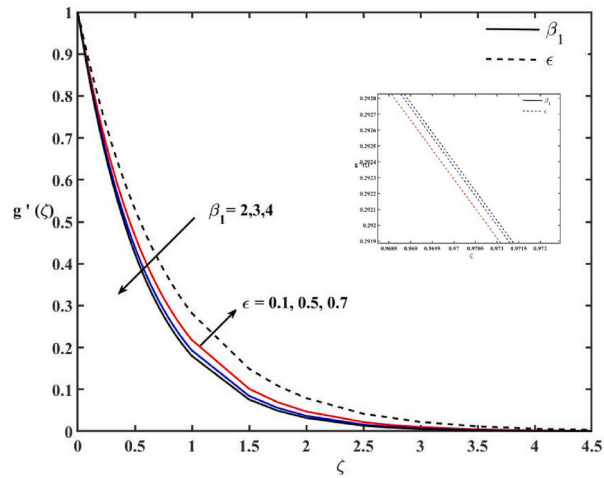


Fig. 5. Effects of \mathcal{E} and β_1 on velocity profile.

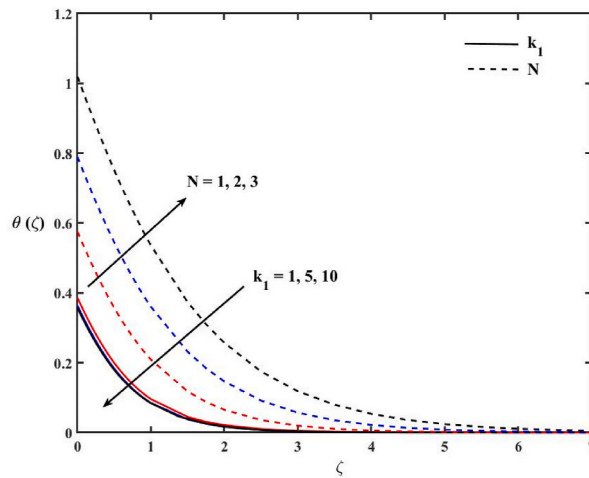


Fig. 6. Effects of N and k_1 on temperature profile.

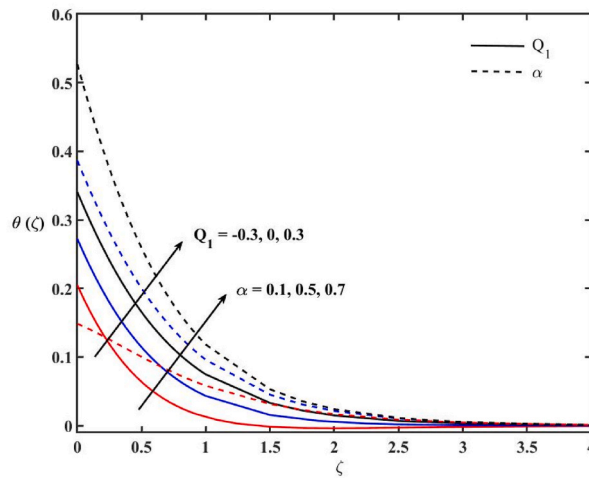


Fig. 7. Effects of Q_1 and α on temperature profile.

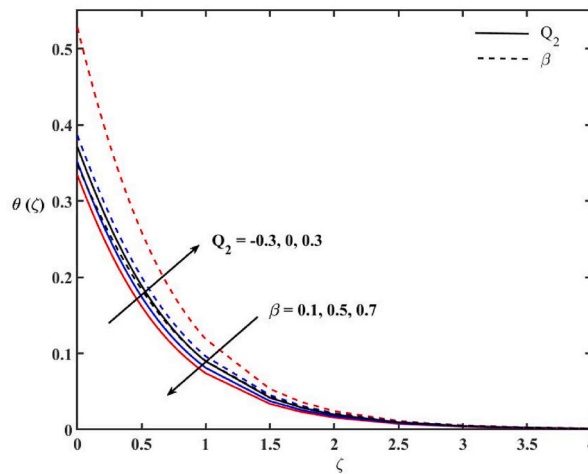


Fig. 8. Effects of Q_2 and β on temperature profile.

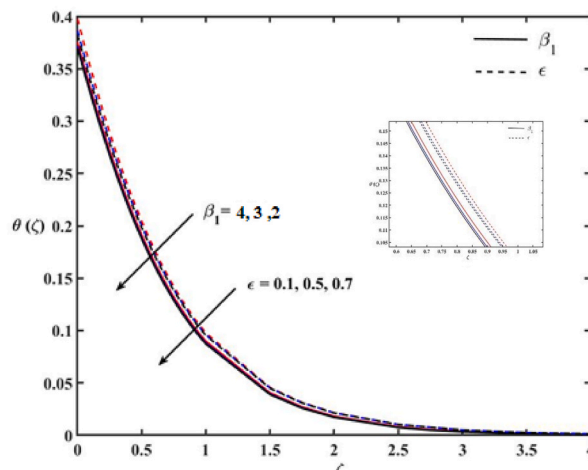


Fig. 9. Effects of \mathcal{E} and β_1 on temperature profile.

case and enhances in the heat generation case. A slight enhancement is observed with the increase of the heat of reaction parameter α . The impacts of Q_2 and β on $g'(\zeta)$ are demonstrated in Fig. 4. It is observed that the impacts of Q_2 are similar to those of Q_1 on the $g'(\zeta)$ as explained in the earlier figure. The increase in the reaction rate β gives a diminution in $g'(\zeta)$, consequently shrinking the momentum boundary layer of the Casson liquid.

Fig. 5 shows the impacts of β_1 and \mathcal{E} on $g'(\zeta)$. The results shown in this figure came in response to a suppression in fluid velocity due to increase in β_1 . An enhancement in β_1 increases the viscosity of fluid, consequently momentum boundary layer thickness and velocity decreases. An insignificant enhancement is observed in the momentum boundary layer with the activation energy parameter (\mathcal{E}).

Fig. 6 indicates the impacts of N and k_1 on the temperature profile $\Theta(\zeta)$. The increase in N enhances $\Theta(\zeta)$. The heat transfer rate reduces with higher k_1 . Hence, to enhance cooling from the stretching surface, the radiation parameter must be fixed low. A slight decrement in $\Theta(\zeta)$ is observed with higher porous medium parameter in the catalytic surface. The impacts of α and Q_1 on $\Theta(\zeta)$ are shown in Fig. 7. The temperature profile enhances when $Q_1 > 0$ and reduces when $Q_1 < 0$. The heat generation parameter increases the temperature of the fluid molecules; consequently, the thermal boundary layer thickness enhances and the heat absorption parameter observes the temperature from the liquid molecules and reduces the thermal boundary layer thickness. The parameter α shows a considerable impact on $\Theta(\zeta)$. The behavior of $\Theta(\zeta)$ is directly proportional to the heat of reaction parameter. The rising value of α increases the thermal boundary thickness. Fig. 8 displays the impacts of Q_2 and β on $\Theta(\zeta)$. The impact of Q_2 on the temperature profile is similar to Q_1 , but it is interesting to note that a good variation in thermal boundary layer is observed with Q_1 . The variation of Q_2 does not show significant variation on the thermal boundary layer. The thermal boundary decreased with the increase of β . The impacts of β_1 and \mathcal{E} on $\Theta(\zeta)$ are exhibited in Fig. 9. It can be seen that an increase in β_1 implicating the higher viscosity of fluid, causes an increase in $\Theta(\zeta)$ as a result of developing an ascending thermal boundary layer. With a larger value of the activation energy parameter (\mathcal{E}), the thickness of the thermal boundary layer decreased slightly.

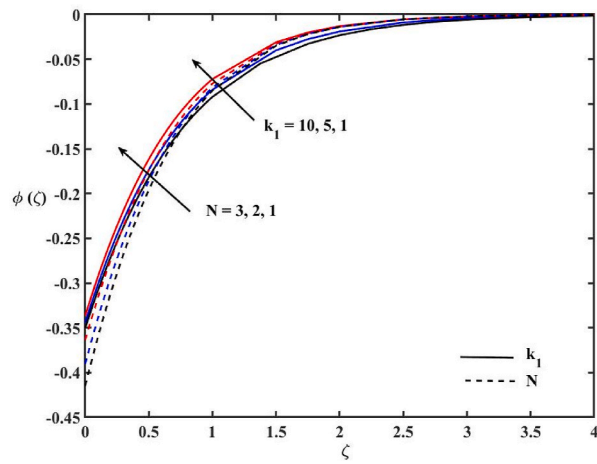


Fig. 10. Effects of N and k_1 on concentration profile.

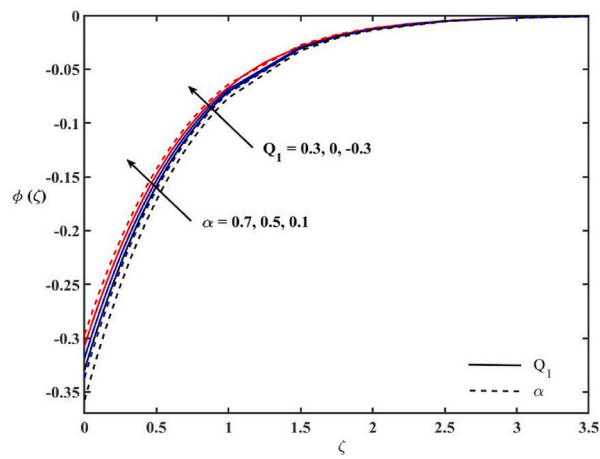


Fig. 11. Effects of Q_1 and α on concentration profile.

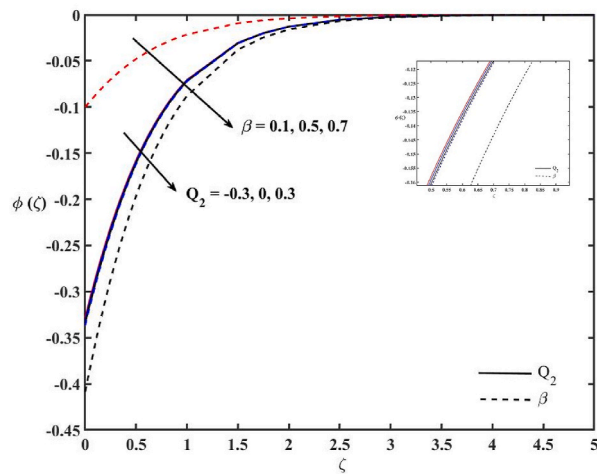


Fig. 12. Effects of Q_2 and β on concentration profile.

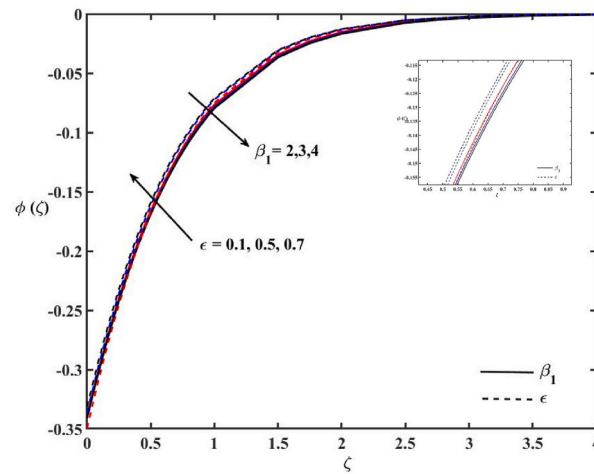
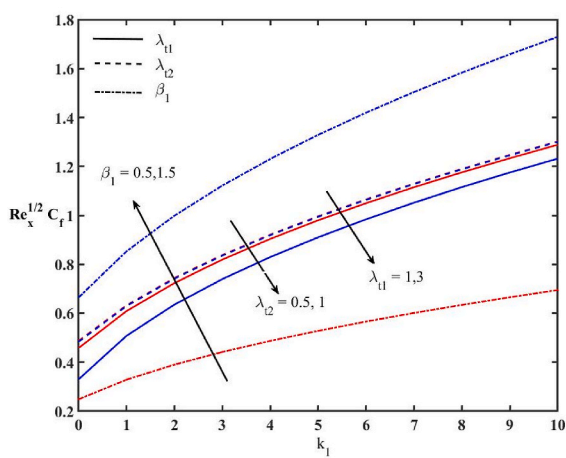
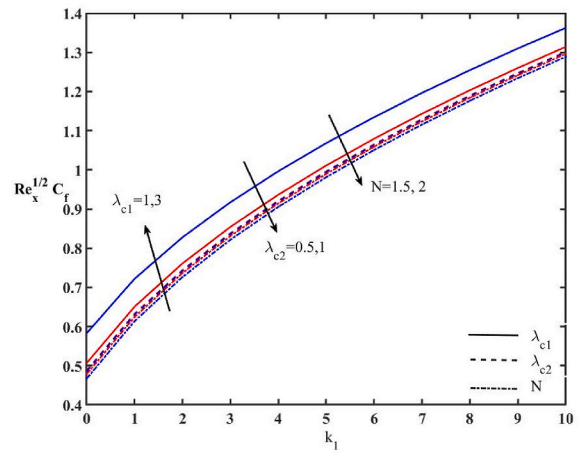


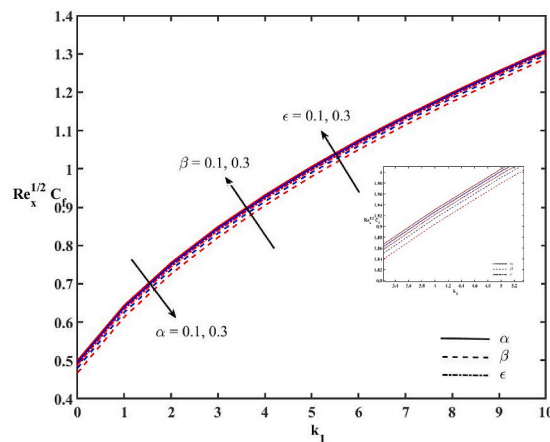
Fig. 13. Effects of ϵ and β_1 on concentration profile.



(a)



(b)



(c)

Fig. 14. Variations of skin friction coefficient (a) Effects of λ_{11} , λ_{12} and β (b) Effects of λ_{c1} , λ_{c2} and N (c) Effects of α , β and ϵ .

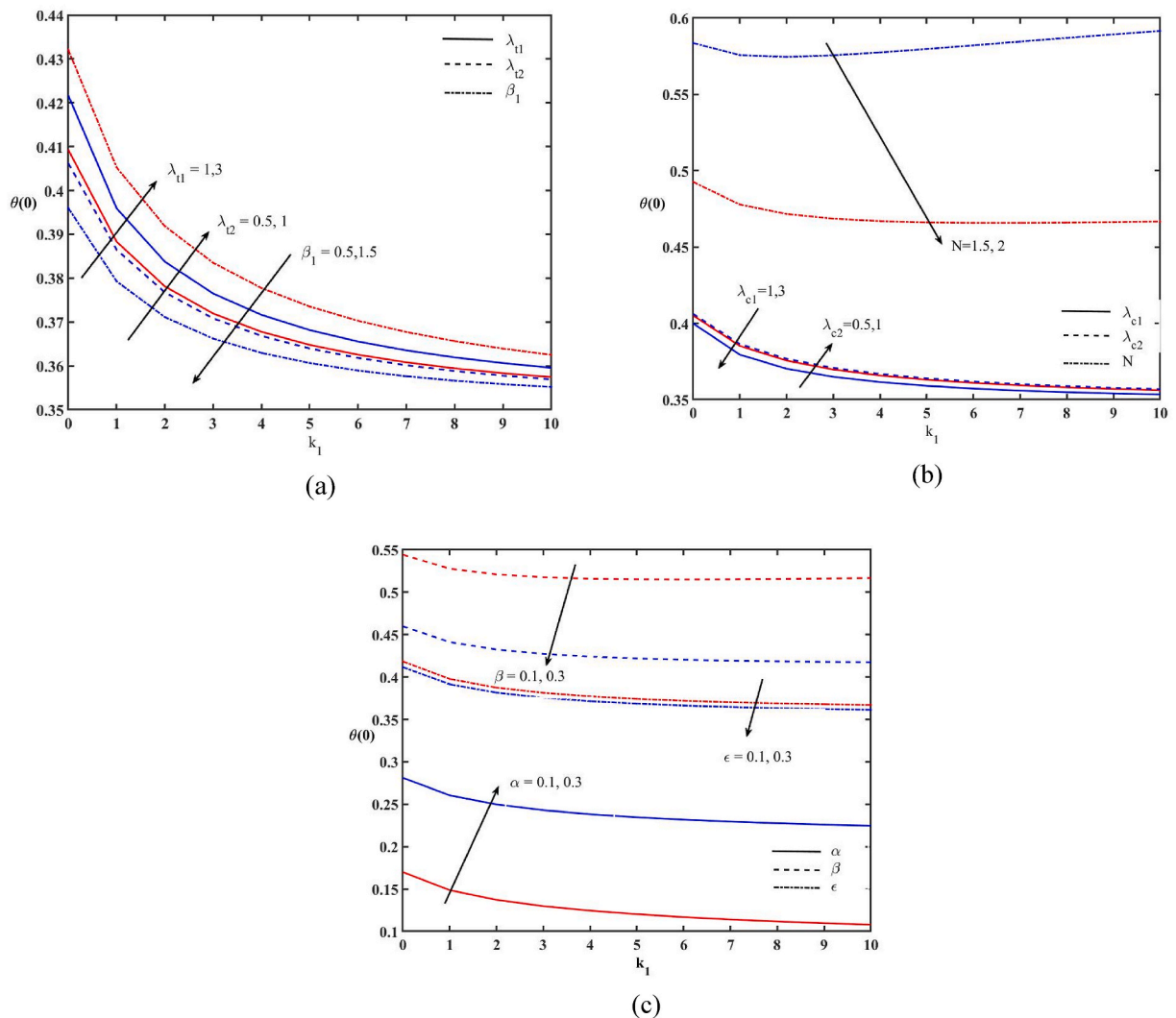


Fig. 15. Variations of non-dimensional wall temperature (a) Effects of λ_{t1} , λ_{t2} and β (b) Effects of λ_{c1} , λ_{c2} and N (c) Effects of α , β and ϵ .

The impacts of N and k_1 on concentration profile $\varphi(\zeta)$ are demonstrated in Fig. 10. It is noted that both N and k_1 raise the concentration profile and reduce the thickness of the concentration boundary layer. Fig. 11 portrays the impacts of Q_1 and α on the concentration profile. The concentration profile increases with α . It is also noted that the concentration profile is higher in the presence of heat generation and lower in the presence of heat absorption. The combined impact of α with heat generation decreases the thickness of the concentration boundary layer. The impacts of β and Q_2 on the concentration profile is examined in Fig. 12. One may note that the temperature dependent heat generation/absorption parameter does not have significant impacts on the concentration profile. The concentration boundary layer increases with the increase of β . Fig. 13 is plotted to show the impacts of β_1 and \mathcal{E} on the concentration profile. It is observed that the increase in β_1 reduces the concentration profile, while \mathcal{E} enhances the concentration profile.

The variations of skin friction coefficient, non-dimensional wall temperature, and non-dimensional wall concentration are depicted in Figs. 14–16 respectively. The skin friction coefficient enhances with the increase of $k_1, \beta_1, \lambda_{c1}, \beta$ and \mathcal{E} ; reduces with $\lambda_{t1}, \lambda_{t2}, \lambda_{c2}, N$ and α (Fig. 14). The increasing values of $\lambda_{t1}, \lambda_{t2}, \lambda_{c2}, \alpha$ increase the non-dimensional wall temperature. The non-dimensional wall temperature decreases with $\beta_1, N, \lambda_{c1}, \beta, k_1$ and \mathcal{E} (Fig. 15). The non-dimensional wall concentration rises with the rising values of $\alpha, \lambda_{t1}, \lambda_{t2}$, and λ_{c2} while it decreases with $\beta, \mathcal{E}, \beta_1, N, k_1$ and λ_{c1} (Fig. 16).

6. Conclusion

The nonlinear mixed convection flow of Casson liquid over a stretching surface is investigated numerically in a porous medium. The Arrhenius kinetics impact is considered at the boundary. The heat and mass transfer are analysed in the presence of space and temperature dependent heat generation/absorption and thermal radiation. The similarity solutions are obtained through the Runge-Kutta

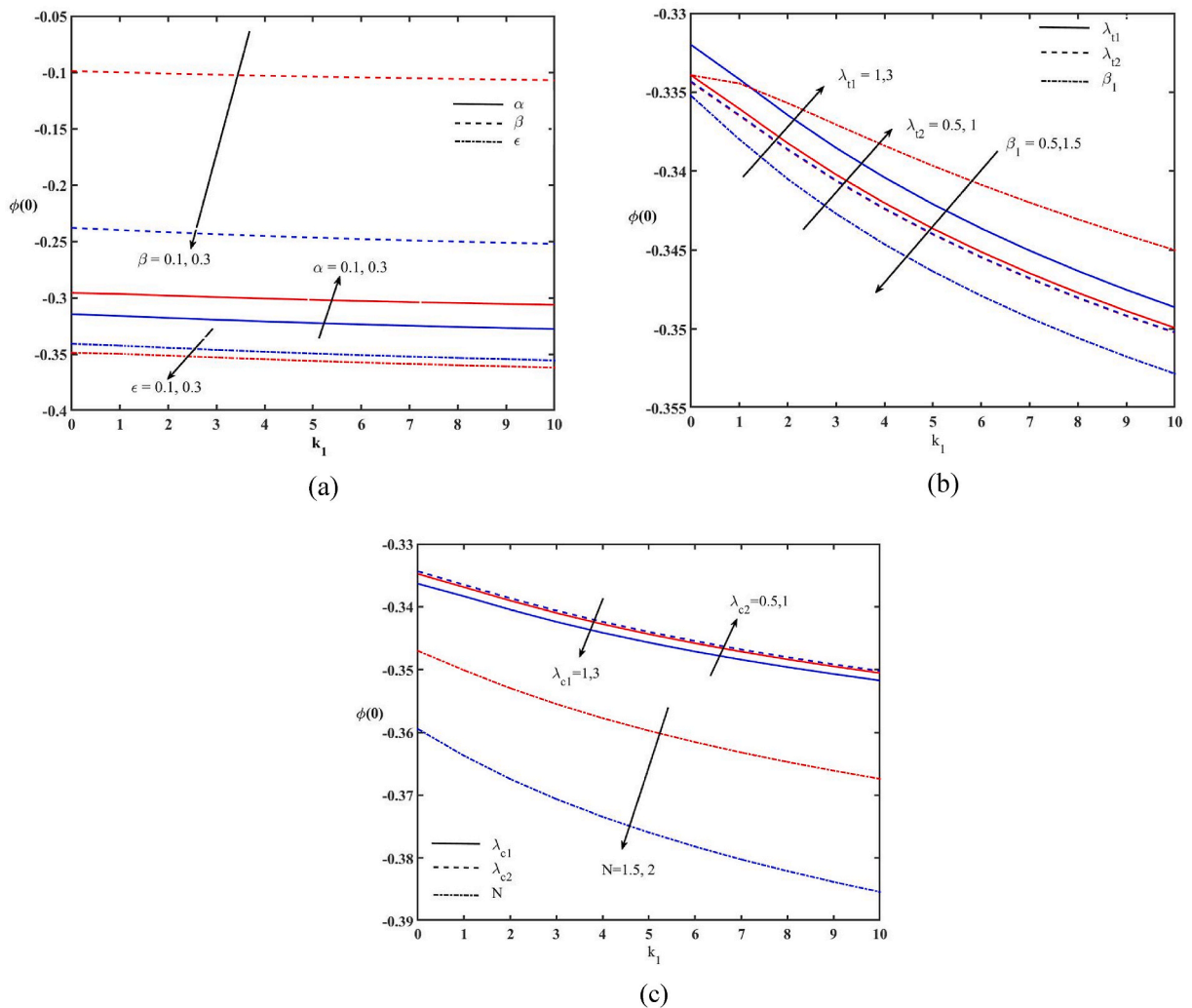


Fig. 16. Variations of non-dimensional wall concentration (a) Effects of λ_{t1} , λ_{t2} and β (b) Effects of λ_{c1} , λ_{c2} and N (c) Effects of α , β and ϵ .

Fhelberg method along with the shooting technique. The key findings of the present study are:

- Enhancing the radiation parameter, space and temperature dependent heat generation, heat of reaction, and activation energy accelerate the velocity profile, while the velocity profile decelerates with the increase of the porous medium parameter, space and temperature dependent heat absorption, reaction rate constant, and Casson parameters in the presence of nonlinear heat and mass transfer and Arrhenius kinetics.
- The temperature profile increases with the increase of radiation, space and temperature dependent heat generation, heat of reaction, and Casson parameters and reduces with the porous medium parameter, space and temperature dependent heat absorption parameter, reaction rate, and activation energy parameters.
- The concentration profile intensifies with the increase of the porous medium parameter, the radiation parameter, space dependent heat generation, heat of reaction, and activation energy, while it reduces with the reaction rate constant, and the Casson parameter.
- The skin friction coefficient enhances with the porous medium parameter, Casson parameter, first order concentration buoyancy, reaction rate, and activation energy parameter and reduces with linear and nonlinear mixed convection due to temperature, and nonlinear convection due to concentration, radiation, and heat of reaction parameters.
- The increasing values of linear and nonlinear mixed convection due to temperature and nonlinear convection due to concentration and heat of reaction increases the non-dimensional wall temperature.
- The non-dimensional wall concentration rises with the rising values of heat of reaction, linear convection and nonlinear mixed convection due to temperature, and nonlinear convection due to concentration parameters.

The current study focused on the heat transmission from an exothermic process to the fluid surrounding it, which drives the

convection flow of Casson fluid in a porous Darcian medium. The future directions of the present study are: the researchers may consider the flow of various non-Newtonian fluids, which is purely driven by the heat supplied to the fluid by an exothermic reaction.

Author contribution statement

N. Vishnu Ganesh; Qasem Al-Mdallal: Conceived and designed the experiments; Performed the experiments; Contributed reagents, materials, analysis tools or data; Wrote the paper. Kalaivanan Raja; Reena K: Analysed and interpreted the data; Contributed reagents, materials, analysis tools or data; Wrote the paper.

Data availability statement

Data included in article/supp. material/referenced in article.

Declaration of competing interest

None.

Acknowledgements

The authors wish to express their sincere thanks to the honourable referees for their valuable comments and suggestions that improved the quality of the paper. Additionally, all authors would like to express their gratitude to the United Arab Emirates University, Al Ain, UAE, for providing financial support with Grant No. 12S122.

References

- [1] A. Atangana, Fractional Operators with Constant and Variable Order with Application to Geo-Hydrology, Academic Press, 2017.
- [2] D.A. Nield, A. Bejan, Convection in Porous Media, vol. 3, Springer, New York, 2006.
- [3] A. Bejan, I. Dincer, S. Lorente, A. Miguel, H. Reis, Porous and Complex Flow Structures in Modern Technologies, Springer Science & Business Media, 2004.
- [4] K. Vafai (Ed.), Handbook of Porous Media, Crc Press, 2015.
- [5] D.B. Ingham, I. Pop (Eds.), Transport Phenomena in Porous Media III, vol. 3, Elsevier, 2005.
- [6] D.B. Ingham, A. Bejan, E. Mamut, I. Pop (Eds.), Emerging Technologies and Techniques in Porous Media, vol. 134, Springer Science & Business Media, 2012.
- [7] A.A. Hakeem, N.V. Ganesh, B. Ganga, Effect of heat radiation in a Walter's liquid B fluid over a stretching sheet with non-uniform heat source/sink and elastic deformation, J. King Saud Univ. Eng. Sci. 26 (2) (2014) 168–175.
- [8] U.S. Mahabaleshwar, I.E. Sarris, G. Lorenzini, Effect of radiation and Navier slip boundary of Walters' liquid B flow over a stretching sheet in a porous media, Int. J. Heat Mass Tran. 127 (2018) 1327–1337.
- [9] M.I. Asjad, R. Ali, A. Iqbal, T. Muhammad, Y.M. Chu, Application of water based drilling clay-nanoparticles in heat transfer of fractional Maxwell fluid over an infinite flat surface, Sci. Rep. 11 (1) (2021) 1–14.
- [10] A.M. Megahed, M.G. Reddy, Numerical treatment for MHD viscoelastic fluid flow with variable fluid properties and viscous dissipation, Indian J. Phys. 95 (4) (2021) 673–679.
- [11] N.V. Ganesh, Q.M. Al-Mdallal, H.F. Öztop, R. Kalaivanan, Analysis of natural convection for a Casson-based multiwall carbon nanotube nanofluid in a partially heated wavy enclosure with a circular obstacle in the presence of thermal radiation, J. Adv. Res. 39 (2022) 167–185.
- [12] S. Manaa, S. Boulaaras, H. Benseridi, M. Dilmi, S. Alodhaibi, Analysis for flow of an incompressible brinkman-type fluid in thin medium with friction, J. Funct. Spaces (2021), 5112840.
- [13] M. Nazeer, F. Hussain, M.O. Ahmad, S. Saeed, M.I. Khan, S. Kadryand, Y.M. Chu, Multi-phase flow of Jeffrey Fluid bounded within magnetized horizontal surface, Surface. Interfac. 22 (2021), 100846.
- [14] U. Habib, T. Hayat, S. Ahmadand, M.S. Alhodaly, Entropy generation and heat transfer analysis in power-law fluid flow: finite difference method, Int. Commun. Heat Mass Tran. 122 (2021), 105111.
- [15] R. Kalaivanan, N.V. Ganesh, Q.M. Al-Mdallal, Buoyancy driven flow of a second-grade nanofluid flow taking into account the Arrhenius activation energy and elastic deformation: models and numerical results, Fluid Dynam. Mater. Process. 17 (2) (2021) 319–332.
- [16] K.M. Ewis, Analytical solution of modified Bingham fluid flow through parallel plates channel subjected to forchheimer medium and Hall current using linearized differential transformation method, J. Adv. Res. Num. Heat Trans. 4 (1) (2021) 14–31.
- [17] R. Razaq, U. Farooq, Non-similar forced convection analysis of Oldroyd-B fluid flow over an exponentially stretching surface, Adv. Mech. Eng. 13 (7) (2021).
- [18] S. Mukhopadhyay, P.R. De, K. Bhattacharyya, G.C. Layek, Casson fluid flow over an unsteady stretching surface, Ain Shams Eng. J. 4 (4) (2023) 933–938.
- [19] N.V. Ganesh, P.K. Kameswaran, A.K. Hakeem, B. Ganga, Second order slip flow of water based nanofluids over a stretching/shrinking sheet embedded in a porous medium with internal heat generation/absorption and thermal jump effects, J. Nanofluids. 8 (3) (2019) 526–542.
- [20] N.V. Ganesh, Q.M. Al-Mdallal, R. Kalaivanan, Exact solution for heat transport of Newtonian fluid with quadratic order thermal slip in a porous medium, Adv. Theory Nonlinear Anal. Appl. 5 (1) (2021) 39–48.
- [21] N.N. Reddy, V.S. Rao, B.R. Reddy, Chemical reaction impact on MHD natural convection flow through porous medium past an exponentially stretching sheet in presence of heat source/sink and viscous dissipation, Case Stud. Therm. Eng. 25 (2021), 100879.
- [22] A.M. Megahed, Improvement of heat transfer mechanism through a Maxwell fluid flow over a stretching sheet embedded in a porous medium and convectively heated, Math. Comput. Simulat. 187 (2021) 97–109.
- [23] S. Ahmad, K. Ali, M. Rizwan, M. Ashraf, Heat and mass transfer attributes of copper–aluminum oxide hybrid nanoparticles flow through a porous medium, Case Stud. Therm. Eng. 25 (2021), 100932.
- [24] I.O. Senge, E.O. Oghre, I.F. Ekang, Influence of radiation on magneto-hydrodynamics flow over an exponentially stretching sheet embedded in a thermally stratified porous medium in the presence of heat source, Earthline J. Math. Sci. 5 (2) (2021) 345–363.
- [25] K. Bhattacharyya, MHD stagnation-point flow of Casson fluid and heat transfer over a stretching sheet with thermal radiation, J. Thermodynamics. (2013), 169674.
- [26] S.A. Shehzad, T. Hayat, A. Alsaedi, Three-dimensional MHD flow of Casson fluid in porous medium with heat generation, J. Appl. Fluid Mech. 9 (1) (2016) 215–223.
- [27] F. Mabood, R.G. Abdel-Rahman, G. Lorenzini, Effect of melting heat transfer and thermal radiation on Casson fluid flow in porous medium over moving surface with magnetohydrodynamics, J. Eng. Thermophys. 25 (4) (2016) 536–547.

- [28] H.R. Patel, Effects of cross diffusion and heat generation on mixed convective MHD flow of Casson fluid through porous medium with non-linear thermal radiation, *Heliyon* 5 (4) (2019), 01555.
- [29] H.R. Patel, Effects of heat generation, thermal radiation, and hall current on MHD Casson fluid flow past an oscillating plate in porous medium, *Multiphas. Sci. Technol.* 31 (1) (2019) 87–107.
- [30] M. Awais, M.A.Z. Raja, S.E. Awan, M. Shoaib, H.M. Ali, Heat and mass transfer phenomenon for the dynamics of Casson fluid through porous medium over shrinking wall subject to Lorentz force and heat source/sink, *Alex. Eng. J.* 60 (1) (2021) 1355–1363.
- [31] R. Nandkeolyar, A.J. Chamkha, A numerical investigation of Hall and radiation effects on MHD three-dimensional Casson fluid flow in a porous medium, *J. Porous Media* 24 (6) (2021) 15–30.
- [32] N.T. Eldabe, M.Y. Abou-Zeid, O.H. El-Kalaawy, S.M. Moawad, O.S. Ahmed, Electromagnetic steady motion of Casson fluid with heat and mass transfer through porous medium past a shrinking surface, *Therm. Sci.* 25 (2021) 257–265.
- [33] H. Ikeda, P.A. Libby, F.A. Williams, J.I. Sato, Catalytic combustion of hydrogen-air mixtures in stagnation flows, *Combust. Flame* 93 (1–2) (1993) 138–148.
- [34] I.K. Puri, Extinction criteria for buoyant nonpremixed flames, *Combust. Sci. Technol.* 84 (1–6) (1992) 305–321.
- [35] B.F. Gray, J.H. Merkin, Thermal explosion: escape times in the uniform temperature approximation. Part 1.—effects of parameter perturbations, *J. Chem. Soc., Faraday Trans.* 86 (4) (1990) 597–601.
- [36] B.F. Gray, J.H. Merkin, Thermal explosion: escape times in the uniform temperature approximation. Part 2. Perturbations of critical initial conditions, *Math. Eng. Ind.* 4 (1) (1993) 13–26.
- [37] B.F. Gray, J.H. Merkin, G.C. Wake, Disjoint bifurcation diagrams in combustion systems, *Math. Comput. Model.* 15 (11) (1991) 25–33.
- [38] M.A. Sadiq, J.H. Merkin, Combustion in a porous material with reactant consumption: the role of the ambient temperature, *Math. Comput. Model.* 20 (1) (1994) 27–46.
- [39] M.A. Chaudhary, J.H. Merkin, Free-convection stagnation-point boundary layers driven by catalytic surface reactions: I the steady states, *J. Eng. Math.* 28 (2) (1994) 145–171.
- [40] J.H. Merkin, M.A. Chaudhary, Free-convection boundary layers on vertical surfaces driven by an exothermic surface reaction, *Q. J. Mech. Appl. Math.* 47 (3) (1994) 405–428.
- [41] M.A. Chaudhary, A. Linan, J.H. Merkin, Free convection boundary layers driven by exothermic surface reactions: critical ambient temperatures, *Math. Eng. Ind.* 5 (2) (1995) 129–145.
- [42] M.A. Chaudhary, J.H. Merkin, Free convection stagnation point boundary layers driven by catalytic surface reactions: II times to ignition, *J. Eng. Math.* 30 (4) (1996) 403–415.
- [43] B.J. Minto, D.B. Ingham, I. Pop, Free convection driven by an exothermic reaction on a vertical surface embedded in porous media, *Int. J. Heat Mass Tran.* 41 (1) (1998) 11–23.
- [44] D.B. Ingham, S.D. Harris, I. Pop, Free-convection boundary layers at a three-dimensional stagnation point driven by exothermic surface reactions, *Hybrid Methods Eng.* 1 (4) (1999).
- [45] J.H. Merkin, I. Pop, Stagnation point flow past a stretching/shrinking sheet driven by Arrhenius kinetics, *Appl. Math. Comput.* 337 (2018) 583–590.
- [46] N.V. Ganesh, R. Kalaivanan, Q.M. Al-Mdallal, K. Reena, Buoyancy driven second grade nano boundary layers over a catalytic surface with reaction rate, heat of reaction and activation energy at boundary, *Case Stud. Therm. Eng.* 28 (2021), 101346.
- [47] L. Zheng, L. Wang, X. Zhang, Analytic solutions of unsteady boundary flow and heat transfer on a permeable stretching sheet with non-uniform heat source/sink, *Commun. Nonlinear Sci. Numer. Simul.* 16 (2) (2011) 731–740.
- [48] W.A. Khan, I. Pop, Boundary-layer flow of a nanofluid past a stretching sheet, *Int. J. Heat Mass Tran.* 53 (11–12) (2010) 2477–2483.
- [49] I. Ullah, S. Shafie, I. Khan, Effects of slip condition and Newtonian heating on MHD flow of Casson fluid over a nonlinearly stretching sheet saturated in a porous medium, *J. King Saud Univ. Sci.* 29 (2) (2017) 250–259.

Nomenclature

C: concentration (kg/m^3)
 C_w : concentration of the sheet (kg/m^3)
 C_∞ : concentration far away from the sheet (kg/m^3)
 C_f : local skin friction coefficient
 c_p : Specific heat capacity ($\text{J}/\text{kg K}$)
 D : molecular diffusivity (m^2/s)
 E : the activation energy (kcal/mol)
 g_1 : acceleration due to gravity (m/s^2)
 k : thermal conductivity ($\text{W}/\text{m K}$)
 k_{ab} : coefficient of mean absorption
 k_p : permeability of the porous medium
 k_1 : porous medium parameter
 N : radiation parameter
 p : pressure ($\text{kg m}^{-1}\text{s}^{-2}$)
 Pr : Prandtl number
 Q_1 : exothermicity of a reaction
 Q_1 : space dependent heat generation/absorption parameter
 Q_2 : temperature dependent heat generation/absorption parameter
 q_f : radiative heat flux
 R : gas constant
 $Re_1^{1/2}$: Reynolds number
 Sc : Schmidt number
 T : local temperature of the fluid (K)
 T_w : temperature of the sheet (K)
 T_∞ : temperature of the fluid far away from the sheet (K)
 u and v : velocity component in x and y direction (m/s)
 u_w : velocity of stretching sheet (m/s)
 x, y : coordinates along and perpendicular to the sheet (m)
 X : reactant
 Y : produce species

Greeksymbols

α : heat of reaction
 β : reaction rate
 β_1 : Casson parameter

β_{t1} : first order thermal expansion coefficient
 β_{t2} : second order thermal expansion coefficient
 β_{c1} : first order solutal coefficient
 β_{c2} : second order solutal coefficient
 σ_{sb} : constant of Stefan-Boltzmann
 ε : activation energy
 ρ : density (kg/m^3)
 g : dimensionless velocity
 θ : dimensionless temperature
 φ : dimensionless concentration
 ζ : dimensionless space variable
 ν : the kinematic viscosity (m^2/sec)
 τ_w : wall shearing stress (N/m^2)
 λ_{t1} : mixed convection parameter due to temperature
 λ_{t2} : nonlinear convection parameter due to temperature
 λ_{c1} : mixed convection parameter due to concentration
 λ_{c2} : nonlinear convection parameter due to concentration